Published in final edited form as:
J Neurophysiol. 2005 May ; 93(5): 2359–2370. doi:10.1152/jn.00533.2004.

Determinants of Spatial and Temporal Coding by Semicircular Canal Afferents

Stephen M. Highstein[1,5], **Richard D. Rabbitt**[2,5], **Gay R. Holstein**[3,5], and **Richard D. Boyle**[4]

[1] Department of Otolaryngology, Washington University School of Medicine, St. Louis, Missouri

[2] Department of Bioengineering, University of Utah, Salt Lake City, Utah

[3] Department of Neurology, Mount Sinai School of Medicine, New York, New York

[4] National Aeronautics and Space Administration Ames BioVIS Technology Center, Moffett Field, California

[5] Marine Biological Laboratory, Woods Hole, Massachusetts

Abstract

The vestibular semicircular canals are internal sensors that signal the magnitude, direction, and temporal properties of angular head motion. Fluid mechanics within the 3-canal labyrinth code the direction of movement and integrate angular acceleration stimuli over time. Directional coding is accomplished by decomposition of complex angular accelerations into 3 biomechanical components—one component exciting each of the 3 ampullary organs and associated afferent nerve bundles separately. For low-frequency angular motion stimuli, fluid displacement within each canal is proportional to angular acceleration. At higher frequencies, above the lower corner frequency, real-time integration is accomplished by viscous forces arising from the movement of fluid within the slender lumen of each canal. This results in angular velocity sensitive fluid displacements. Reflecting this, a subset of afferent fibers indeed report angular acceleration to the brain for low frequencies of head movement and report angular velocity for higher frequencies. However, a substantial number of afferent fibers also report angular acceleration, or a signal between acceleration and velocity, even at frequencies where the endolymph displacement is known to follow angular head velocity. These non-velocity-sensitive afferent signals cannot be attributed to canal biomechanics alone. The responses of non-velocity-sensitive cells include a mathematical differentiation (first-order or fractional) imparted by hair-cell and/or afferent complexes. This mathematical differentiation from velocity to acceleration cannot be attributed to hair cell ionic currents, but occurs as a result of the dynamics of synaptic transmission between hair cells and their primary afferent fibers. The evidence for this conclusion is reviewed below.

INTRODUCTION

The vestibular system is phylogenetically ancient. Its development was an important evolutionary event, enabling vertebrates (and invertebrates) to maintain equilibrium and spatial orientation while moving freely in their environments. Optimization of the vestibular end-organ plan in vertebrates occurred rapidly, as evidenced by the close similarity between the labyrinths of the fossil record, the earliest extant species, such as myxine and lamprey,

Address for reprint requests and other correspondence: S. M. Highstein, Washington University School of Medicine, Department of Otolaryngology, St. Louis, MO 63110..

and those of human and nonhuman primates. Thus the original design was successful in accomplishing its goals and has changed little throughout phylogeny.

The vestibular labyrinths sense and report angular and linear accelerations of the head. There are 5 paired labyrinthine end organs, consisting of 3 angular and 2 linear accelerometers. The angular accelerometers, the semicircular canals, are the subject of this review. In primates, the lateral (horizontal) canal is positioned in the head to align roughly with the head-based yaw axis of rotation, whereas the anterior and posterior canals are situated in the orthogonal planes, each oriented approximately 45 deg from the pitch and roll axes of rotation. Each semicircular canal is an endolymphatic fluid-filled tube with an enlarged sac called an *ampulla* at one end. The receptor sheet, the crista ampullaris, is found inside the sac and is anchored to the ampullary wall. The crista itself is an inverted saddle-shaped structure whose topmost layer consists of a single sheet of sensory hair cells. The apical hairs or cilia of these cells can reach 100 microns in length, and they project into a gelatinous vane or cupula that closes the ampullary space to transcupular fluid flow. Vestibular afferent nerves are in contact with the hair cells, and emerge from the base of the ampulla to travel toward the brain.

Because the labyrinths are tethered to the skull, the canals move with the head. Angular acceleration of the head generates an inertial force within the endolymph. Displacement of the endolymph produces a viscous drag force on the canal walls and a compensatory displacement of the cupula and ciliary bundles, which generates an elastic restorative force. These forces balance the inertial force in dynamic equilibrium (Curthoys and Oman 1987; Damiano and Rabbitt 1996; Lorenté de Nó 1927; Steinhausen 1933; Van Buskirk et al. 1976). Deflection of the stereocilia leads to the generation of a receptor potential in the hair cell, ultimately resulting in the modulation of transmitter release from the hair cells. Individual primary vestibular afferent fibers typically receive and summate input from multiple hair cells (Boyle et al. 1991; Goldberg 2000; Lysakowski and Goldberg 1997; Lysakowski et al. 1995). Summated depolarizations generate action potentials in the afferents that encode parameters of angular head velocity and acceleration. These parameters are transmitted to the brain stem by the frequency and relative timing of the action potentials.

The macromechanical transduction mechanisms noted above, and the modulation of semicircular canal primary afferent responses resulting from head rotation are remarkably similar among vertebrates (Blanks et al. 1975; Boyle and Highstein 1990; Dickman and Correia 1989a,b; Fernandez and Goldberg 1971; Goldberg and Fernandez 1971b; Landolt and Correia 1980; Lowenstein and Sand 1940; O'Leary and Dunn 1976). This physiological invariance can be attributed to the similarity in gross structure of the labyrinth across species (Curthoys and Oman 1987; Igarashi 1966; Igarashi and Yoshinobu 1966; Wersäll and Bagger-Sjöbäck 1974). Indeed, the membranous labyrinth of the toadfish, *Opsanus tau*, is remarkably similar in size and shape to that of modern man. Because of this gross anatomical invariance across species, the physical principles underlying the macromechanics of angular motion transduction by the semicircular canals are nearly identical across many species (reviewed by Rabbitt et al. 2004).

The endolymphatic fluid displacement resulting from angular head acceleration can be reproduced by mechanical indentation of the long and slender canal, an experimental strategy that Ewald (1892) invented, applying a pneumatically actuated tapered rod to compress the membranous canal duct mechanically. More recently, Dickman et al. (Dickman and Correia 1989a; Dickman et al. 1988) applied a piezoelectrically driven rod to the pigeon canal, and demonstrated that the neural response dynamics attributed to rotational stimuli are generally reproduced by mechanical indentation. Rabbitt et al. (1995) further

documented the utility of this method by quantifying and modeling the results of indentation. In these studies, a single flat-ended glass rod of about the same dimension as the canal diameter was placed in contact with the canal limb, about 3–7 mm from the sensory epithelium, at a site where the canal is backed by bone. A static preload was set by stimulating with a sinusoidal profile of indentation (peak-to-peak displacement) and lowering the rod until the afferent nerve response indicated continuous contact by the indenter rod. This procedure serves to linearize subsequent stimuli about the preload indentation. Theory, verified by experimental results, indicates that the responses of semicircular canal afferents to head rotation can be mimicked by canal limb mechanical indentation over a broad range of physiological frequencies (Rabbitt et al. 1995). Linearity of the first harmonic afferent response to indentation was also established. However, the fluid dynamics induced by indentation begin to diverge from those induced by head rotation at stimulus frequencies >2 Hz. This is because at high frequencies inertial forces on the fluid become dominant, causing a cutoff in the biomechanical response to head rotation, the classical upper corner. In contrast, at higher frequencies of mechanical stimulation, the indenter forces endolymph flow, simply overpowering the additional inertial force. Therefore when using mechanical indentation stimuli at frequencies >2 Hz, the amplitude of indentation must be decreased and the phase must be retarded to achieve the same movements of the cupula and endolymph as are produced by head rotation (Rabbitt et al. 1995).

Substituting canal indentation for angular rotation, a strategy that we have used extensively, facilitates experiments requiring stable intracellular recordings from hair cells or nerve fibers. Figure 1 indicates the placement of the indenter on the long and slender limb of the horizontal canal in the oyster toadfish *Opsanus tau* (Fig. 1, HCI). In this preparation, one micron of canal indentation is equivalent to approximately 4°/s angular velocity, at least at low frequencies. As noted, mechanical indentation stimuli, like physiological rotation, modulate hair cell transduction currents by inducing micromechanical stereociliary bundle displacements and corresponding nanomechanical gating of ciliary bundle ion channels. The open probability of hair cell transduction channels is a function of bundle deflection and determines the ion flow through these channels. Based on data from other hair cell organs, about 13% of the transduction channels are open when the bundle is not moving, resulting in a resting rate of current flow (Hudspeth 1989a,b,1997). Hair cell receptor potentials and afferent responses can be modulated experimentally by applying transepithelial electrical stimuli or by voltage clamping the endolymph relative to the perilymph (Fig. 1, I_e) (Damiano and Rabbitt 1996;Highstein and Politoff 1978;Norris et al. 1998). The latter manipulation modulates the apical-face membrane potential and causes current flow through open transduction channels in the absence of an applied mechanical force on the hair bundles. Although hair bundle motion in the otolith organs is known to be elicited by transepithelial electrical polarization (Bozovic and Hudspeth 2003), in the canals the mechanical movement is relatively small and a majority of the induced afferent responses appear to arise from alterations in the current flow through open transduction channels by modulation of the apical face membrane potential (Highstein et al. 1996). This electrical stimulus also activates synaptic transmitter release from hair cell basal synapses. We have used this strategy to activate hair cells in the absence of biomechanical stimulation of the canal [cf. Fig. 1 illustrating the loci for measurement of translabyrinthine potentials (V_e), recordings of single canal afferents (V_n), and hair cell voltage- and current-clamp recordings ($HC_{VC/CC}$)].

To record hair cell potentials and currents in vivo, quartz microelectrodes can be introduced by a small fistula or opening in the utricular side of the horizontal canal ampulla (Fig. 1, $HC_{VC/CC}$) to impale hair cells during canal indentation. Control experiments have verified that the mechanical stimulus is dominated by the long and slender limb of the canal (Rabbitt

et al. 1995), which is on the canal side of the cupula, so that the presence of the fistula (on the utricular side) has no impact on the effectiveness of the stimulus. Indeed, recordings from afferents remain stable and unchanged after fistulation and after resealing of the fistula (S. M. Highstein and R. D. Boyle, unpublished data). Further, the fistula is effectively sealed in these experiments by the interface pressure between endolymph and FC-75 (3M), a fluorocarbon that is used to fill the perilymphatic space. It should be noted that the toadfish is the only vertebrate preparation used to date that allows intracellular recordings from vestibular hair cells in vivo. This offers the experimental potential to directly relate the intracellular hair cell recordings to data from the vestibular nerve, which provides a reference regarding the total output of the vestibular peripheral sensory apparatus, including all signal processing performed by the labyrinthine canal end organ.

RESPONSES OF AFFERENT NERVES: BODE PLOTS

Activation of hair cells by rotation, indentation, or endolymphatic polarization evokes postsynaptic potentials that may lead to impulses in primary afferent fibers (Smotherman and Narins 2000). Individual semicircular canal afferents exhibit a wide range of temporal responses across the frequency spectrum of head movements. Such responses define the *response dynamics* of the afferent, a term that is generally used to indicate the first harmonic of afferent modulation, reported in terms of gain (e.g., impulses/s per degree/s) and phase (e.g., degree re: stimulus peak), referenced to the sinusoidal angular velocity of the head or displacement of the mechanical indentation stimulus. Figure 2 illustrates gain and phase responses. Figure 2, *A* and *B*, shows the responses of 2 different afferents to the angular velocity stimulus portrayed in Fig. 2*C*. A_1 and B_1 represent the instantaneous spike frequencies; spikes are illustrated in A_2 and B_2. By comparing the 2 types of afferent responses, it is clear that spike modulation in *B* is small, whereas that in *A* is more substantial. In addition, the peak modulation in afferent *B* is “in phase” with velocity, but is shifted toward acceleration (a phase lead of about 50°) in *A*. The measurements in Fig. 2 can be repeated at several different stimulus frequencies and then plotted in the Bode form of gain and phase (Fig. 3). Although afferent dynamics in the toadfish form a response continuum, responses can be discussed in terms of 3 broad qualitative groups of fibers (Boyle et al. 1991; cf. Figure 3): *1*) low gain (LG) velocity-sensitive; *2*) high gain (HG) velocity-sensitive; and *3*) acceleration-sensitive (A) afferents. LG afferents respond nearly linearly across the range of physiological amplitudes and frequencies and have Bode plots for angular velocity stimuli indicative of a simple high-pass filter. Differences between individual LG units are manifest primarily in overall gain (sensitivity) (Boyle et al. 1991). HG and A afferents also have a range of amplitudes over which their responses are nearly linear, but express a much richer set of response dynamics showing a wide range of gain and phase enhancements as the stimulus frequency is increased.

Response dynamics similar to the LG and HG afferents of fish are expressed by canal nerves in many vertebrate species (Blanks et al. 1975; Curthoys 1982; Estes et al. 1975; Goldberg and Fernandez 1971a,b, 1975; Goldberg et al. 1992; Honrubia et al. 1981; Hullar et al. 2005). However, the pure acceleration-sensitive afferents, which are in phase with acceleration across the entire bandwidth of rotary stimulation from 0.005 to 10 Hz and above, appear to be unique to lower vertebrates.

MORPHOPHYSIOLOGY

To correlate the differences in response dynamics with morphologic attributes of the crista, individual afferent fibers of several species have been identified by response class (as described above) and injected with tracer compounds for subsequent anatomical analysis (Baird et al. 1988; Boyle et al. 1991; Brichta and Goldberg 2000; Fernandez et al. 1988,

1995; Honrubia et al. 1989; Lysakowski and Goldberg 1997; Lysakowski et al. 1995; O'Leary et al. 1974; Schessel et al. 1991). The toadfish provides an example of a teleost with a simplified crista, in that anamniotes (fish and amphibians) possess only Type II hair cells, and have no Type I cells or calyx afferent endings.

Figure 4 illustrates semicircular canal hair cells, intracellularly injected with Neurobiotin after recording (sample records from the heavily labeled cell are shown in Fig. 4*D*). It is worthy of note that the stereociliary bundle is filled with tracer to about 20 μM from the apex of the hair cell. A "dot" (small sphere) of label can also be seen above the cell in the rotated images shown in Fig. 4, *B* and *C*. Semicircular canal hair cells are notable because of their long stereociliary bundles that can reach 100 μm in length. We can speculate that if the tracer traveled up the bundle and into the cupula by open transduction channels, then these channels were present only in the shorter cilia. We hypothesize that these shorter cilia, perhaps ≤20 μm in length, contain the transduction channels, whereas the taller members of the bundle serve to anchor the cilia within the fibrous matrix of the cupula but do not contain transduction channels.

Figure 5 *A* is a surface map of the toadfish crista illustrating the locations of afferent dendrites bearing terminals of LG, HG, and A afferents (Boyle et al. 1991). Note that LG afferents are confined to the lateral extremes of the long axis of the crista, whereas HG and A afferents intermingle more centrally, spanning the entire extent of the short axis of the receptor sheet. In the chinchilla crista, a common mammalian vestibular subject (Baird et al. 1988; Fernandez et al. 1988), canal afferents have been typed as calyx-only, bouton-only, and dimorphic endings, so named by Schessel et al. (1991) because this class of afferent contacts both Type I cells by a calyx ending and Type II cells by bouton endings. Physiologically, calyx units are the most phase advanced, but have gains in between those of the highest gain dimorphic units and the bouton units. Dimorphic units are the most common, have widely diverse gains, but also exhibit complex dynamics including high-frequency phase and gain enhancements. Boutononly units have the lowest gains, are generally in phase with the velocity of stimulation, and do not exhibit marked gain and phase enhancements at high frequencies of stimulation. Therefore mammalian bouton units are physiologically similar to fish LG afferents, whereas dimorphic afferents resemble HG fish afferents. Calyx-only cells, not present in fish, are distinguished by their lower gains and higher phase advances.

The morphophysiology of chinchilla and squirrel monkey canal afferents has been extensively studied by Goldberg and colleagues and has recently been fully reviewed and documented by Lysakowski and Goldberg (2004). Figure 5, *B–D* are surface maps of the chinchilla crista that plot the locations of calyx (*B*), dimorphic (*C*), and bouton afferents (*D*). In contrast to the linear organization of the fish crista, the chinchilla crista has a concentric organization of central, intermediate, and peripheral zones. Calyx-only units are limited to the central zone (*B*) and bouton-only units are restricted to the peripheral zone (*D*). Dimorphic afferents are spread throughout all 3 zones (*C*), but with a relative paucity in the central region. Interested readers are referred to Baird et al. (1988), Fernandez et al. (1988), and Lysakowski and Goldberg (2004) for more detailed descriptions.

Although it is possible for a differential motion profile of the central and peripheral regions of the canal cupula (Damiano 1996; Silver et al. 1998; Yamauchi et al. 2002a) to contribute to differential response dynamics in fish, in mammals the concentric organization of the crista precludes this.

REGULARITY OF AFFERENT DISCHARGE

Primary afferent interspike interval discharge, normalized as CV* (Goldberg et al. 1984), has been shown to correlate with some measures of diversity in afferent response dynamics. However, these correlations are not universal, even in mammals, and do not extend to all species (Boyle and Highstein 1990; Honrubia et al. 1981). Walsh et al. (1972) conclude that morphologic features of vestibular fiber termination patterns are unlikely to be causal determinants of fiber regularity or response dynamics, and this same lack of relationship has been demonstrated in the auditory (Liberman 1982) and somatosensory systems (Johansson and Valbo 1983). The interested reader is referred to Hille (1992) and Kernell (1968) for discussions of the cellular mechanisms leading to regularity of discharge. We concur with Goldberg et al. (Fernandez et al. 1990) that the diversity of response dynamics seen in vestibular primary afferents is not causally related to afferent interspike discharge regularity. In our view, regularity is conferred on afferents by virtue of the intrinsic ionic channel composition resident within postsynaptic structures, most likely at the impulse initiation zone. Finally, possible effects of the recently discovered diversity of transmitter phenotypes in crista (Holstein et al. 2004b,c) on afferent regularity have not yet been explored.

ADAPTATION OF AFFERENT NERVES

Steps of angular acceleration evoke diverse responses that are expressed in the time course and extent of afferent adaptation in all species studied to date. Reptiles, birds, and fish all have adapting semicircular canal afferents similar to those in toadfish (Boyle and Highstein 1990; Brichta and Goldberg 1996; Dickman and Correia 1989b; Fernandez and Goldberg 1971; Honrubia et al. 1989; O'Leary and Dunn 1976; Rabbitt et al. 2004a). Adaptation time constants in mammals are lower on average, but are still quite significant in some afferents (Baird et al. 1988; Fernandez and Goldberg 1971; Goldberg and Brichta 1998; Goldberg et al. 1990; Hullar et al. 2004). Thus results of afferent adaptation studies in fish appear to have broad relevance for vertebrate species. Figure 6 illustrates 2 representative afferent nerve responses in toadfish (A_1 and B_1) to excitatory and inhibitory square-wave stimuli (A_3, B_3) (Rabbitt et al. 2005). Afferent adaptation is asymmetric for excitatory versus inhibitory stimuli. For excitatory stimuli, adaptation follows a time course that can be described by a double-exponential curve with 2 time constants: a relatively fast adaptation (τ_f) immediately after onset of the step, followed by a slow adaptation (τ_s). This 2-time-constant response for excitatory steps is apparent in the initial rapid adaptation and subsequent slow recovery adaptation seen in B_1. This unit also clearly exhibits nonlinear inhibitory cutoff (B_1, zero firing region) where the firing rate decreases to zero. For units that do not cut off during inhibitory stimuli, adaptation follows a single-exponential curve with a time constant equal to that of the slow adaptation observed during excitatory stimulation (A_1, τ_s). This asymmetric nonlinearity reflects a fast adaptation process in response to excitatory stimuli that is absent, or obscured, during inhibitory stimulation.

Afferent adaptation time constants in fish are summarized in Fig. 6 (*right*), and are well described by a log-normal distribution with the total response times spanning approximately 6 orders of magnitude (about 10^{-3} to 10^{3} s; $n = 46$). Although a most probable adaptation time can be identified for each afferent, the slowest adaptation times of the population cannot be determined because of the technical difficulty inherent in recording from units for such prolonged time periods. Because the canal lumen is plugged in these experiments, the adaptation times are not associated with the mechanical time constant of the canal–the displacement of the cupula is nearly constant throughout the adaptation process.

SOURCES OF AFFERENT RESPONSE DIVERSITY

Thus the neural responses of individual vestibular afferent fibers are diverse. Canal morphology can be used to distinguish 5 broad stages of information processing from head acceleration to the specification of the frequency code carried by the VIIIth nerve: *1*) biomechanics, including cupular and hair bundle motions and their antecedents; *2*) the mechano-transduction process performed at the sensory hair bundle and apical hair cell regions; *3*) voltage-sensitive basolateral hair cell currents that may shape the receptor potentials produced by transduction; and the synaptic complex present at the base of each hair cell, including both *4*) pre- and *5*) postsynaptic factors.

Biomechanics

The fundamental role of semicircular canal biomechanics in shaping temporal response dynamics and directional sensitivity has been recognized since the late 1800s (Camis 1930). Figure 7 illustrates the role of semicircular canal mechanics in transforming angular head accelerations into displacements of sensory hair cell cilia. Endolymph displacement within the 3-canal labyrinth is responsible for decomposing the 3-dimensional direction of angular head motion into 3 separate vector components associated with the planes of the individual canals. The fluid volume displacement within each canal is maximal for a specific direction of angular acceleration, as indicated for the lateral canal by the arrow (Fig. 7*A*, Max). Rotations orthogonal to the maximal response direction do not induce fluid motion and thereby define the null plane of the canal (Fig. 7*A*) (Blanks et al. 1985; Dickman 1996; Estes et al. 1975; Reisine et al. 1988). Rotations in directions between the null plane and the maximal response direction evoke gains that obey a simple cosine dependency, illustrated for the lateral canal by the green spherical “bubbles” (Fig. 7*A*) (Rabbitt et al. 1999). This biomechanical decomposition underlies directional coding by the semicircular canals.

The role of canal mechanics in *temporal* coding is exemplified by the relationship between cupular volume displacement and angular frequency of head motion (Curthoys and Oman 1987; Lorenté de Nó 1927; Steinhausen 1933; Van Buskirk et al. 1976). Figure 7*B* illustrates the magnitude of cupular volume displacement (*B*) and phase (*C*), both relative to peak angular head velocity. In both parts of the figure, typical mammalian responses are plotted as thick solid curves (Fernandez and Goldberg 1971; Rabbitt et al. 2004). The most physiologically relevant range of frequencies falls in the mid-band, where the volume displacement of the cupula is proportional to, and in phase with, angular head velocity. Within this critical frequency range, the viscosity of the endolymph within the membranous labyrinth is responsible for temporal integration of angular head acceleration to generate cupular displacements proportional to angular head velocity. It is interesting to note that increasing the size of the labyrinth does indeed increase sensitivity, but at the expense of bandwidth (reviewed by Rabbitt et al. 2004). Relatively flat gain and phase responses across the frequency spectrum have obvious advantages in neural control systems such as the vestibuloocular reflex, where compensatory eye movements are required to stabilize the visual image on the retina over a wide bandwidth of head movements. It seems likely that the bandwidth advantage may have contributed to the evolution of a relatively small labyrinth, particularly obvious in species such as the cetaceans [an evolutionary view that contrasts with the reduced-sensitivity hypothesis that has been advanced recently (Spoor et al. 2002)].

Finally, endolymph volume displacements are converted to a form that is appropriate for activation of sensory hair cells by the cupula. The cupula is a hydrated gel that overlies the sensory epithelium and spans the entire cross section of the ampulla. Experimental observations by Hillman and McLaren (1979) and Yamauchi et al. (2002b) clearly show a diaphragm-like displacement of the cupula, at least at low stimulus frequencies. This is

illustrated in Fig. 7*D* using predictions from a simple finite-element model of the cupula (Yamauchi et al. 2002a,b). Although the maximum cupular displacement occurs near the geometric center of the ampulla, the maximum shear strain occurs precisely at the level where the sensory hair bundles project into the cupula (Fig. 7*E*). Because it is the relative displacement between adjacent cilia that ultimately leads to transduction channel gating, the shear strain in the cupula appears to be ideally suited to activate the hair cells. At low frequencies, the shear strain is proportional to, and in phase with, the cupula volume displacement such that cupular micromechanics are not a significant factor in determining semicircular canal afferent temporal response dynamics. Theoretical considerations indicate that there may be some temporal contribution at stimulus frequencies ≳5 Hz in humans (Damiano 1996), but this effect is predicted to be small in comparison to nonmechanical factors shaping afferent responses, as discussed in the following text.

Hair-cell transduction

VOLTAGE CLAMP—Micromechanical ion channels within the hair bundles open or close when the bundles move, thereby allowing ionic currents to flow and creating receptor potentials in the hair cells. To study this process, toadfish hair cells were impaled in vivo with sharp microelectrodes and records were obtained in bridge-, current-, or voltage-clamp mode using a discontinuous single microelectrode switch clamp switching at about 33 kHz (Highstein et al. 1996). Figure 8 *A* illustrates sample records in voltage (8*A*, *bottom*) and current (8*A*, *top*) clamp. Figure 8*B* illustrates the average phase advance re: velocity of afferent nerve response, for comparison to those of hair cells in current and voltage clamp. It is evident from Fig. 8*B* that the range of the phases re: velocity seen in the hair cell voltage-clamp records falls far short of the wide range of afferent nerve response phases (Holstein et al. 2004a; also cf. Figs. 7 and 9 in Rabbitt et al. 2004). In general, Bode plots of hair cell responses (phase and gain re: indentational frequency) evidence rather flat dynamics (Highstein et al. 1996). These flat dynamics are also seen in the responses of the canal microphonic to indentational sweep stimuli (Fig. 8; Rabbitt et al. 2004). The microphonic reflects the summed activity of all of the hair cells in the stimulated canal. That these microphonic dynamics are flat across the frequency band from 0.5 to 20 Hz validates the conclusion derived from single-cell recordings. Considering the relatively broad span of the phases of nerve responses expressed in *afferent* Bode plots (from velocity to acceleration, Fig. 3), the limited phase advances in the hair cell receptor potentials are remarkable. This disparity indicates that hair cell current/voltage responses do not reflect the broad range of afferent dynamics and thereby implicate a later stage of transduction as the major site of afferent response diversity.

CURRENT CLAMP (BASOLATERAL CURRENT CONTRIBUTIONS TO AFFERENT DYNAMICS)—Theoretically, the voltage-sensitive channels present in basolateral hair cell membranes could cause hair cell responses to bundle motion recorded in current clamp to have temporal responses that differ significantly from responses recorded in voltage clamp. However, comparison of the current- and voltage-clamp phases in Fig. 8 leads to the conclusion that basolateral currents shift hair cell receptor potentials only a small amount relative to the transduction currents. The average phase of the voltage-clamp records was −8° re: velocity, whereas the current-clamp records were advanced +11° (Fig. 8). In contrast, the average afferent phase was 50° advanced and ranged from −50 to +150°. We conclude that basolateral hair cell currents play some role, but are not the critical feature shaping afferent dynamics, a conclusion also reached by other investigators (Goldberg and Brichta 2002).

HAIR-CELL ADAPTATION—To further investigate the origins of afferent response diversity, the time course of hair cell adaptation was compared with that of the afferents

(Fig. 6). Adaptation times of hair cells were well described by a log-normal distribution with a mean of 112 s (SD 3.16 s). Hair cell transduction current adaptation, if present at all, was quite small relative to the adaptation of afferent firing rates, at least over the physiological bandwidth tested. This observation also held true for hair-cell receptor potentials. It should be noted that step bundle motion rise time in this paradigm was too slow to reveal the fast adaptation noted in reduced preparations (Crawford et al. 1989;Fettiplace and Ricci 2003;Kennedy et al. 2003; Ricci et al. 1998,2000;Wu et al. 1999) and that experimental limitations preclude the extended intracellular hair cell recording times that might reveal very slow adaptation. Nevertheless, there were major differences between hair cell and afferent adaptation time constants. Adaptation times of hair cells and afferent nerves both followed log-normal distributions, but the hair cell mean was at least 2 orders of magnitude slower than that of the afferent nerves. Thus we conclude that the dynamic range and bandwidth of adaptation and frequency response dynamics present at the level of afferent discharge are not present at the level of hair-cell current or voltage. (Note that that these conclusions are based on experiments performed in fish lacking Type I hair cells. We hypothesize that similar results will also be true in mammals, although this has yet to be tested experimentally.)

Although it seems somewhat counterintuitive that a mechanoreceptor would use synaptic transmission, rather than intrinsic biomechanics, to shape its responses to mechanical stimuli such as angular acceleration, this seems to be the inevitable conclusion. In fact, striking differences are observed in the temporal responses of pre- and posttransduction components of the signal processing cascade, up to and including the hair-cell basolateral currents, in comparison with the responses of primary afferent neurons.

The diverse temporal responses of afferents to step and sinusoidal stimuli versus the uncomplicated responses of the hair cells argues in favor of substantive signal processing at the synapses between hair cells and afferents. The flat gain and phase of hair cells over the bandwidth tested is somewhat surprising, but is notable because our experiments have been conducted in vivo and the stimuli are restricted to naturally occurring physiological levels and rates. Hair cells hardly adapt, whereas afferent adaptation spans several orders of magnitude (Holstein et al. 2004a). Previous data indicate that the extent of slow adaptation in hair cells may be reduced as the stimulus magnitude is decreased to the physiological range (Holt et al. 1997; Shepherd and Corey 1992, 1994). The present experiments were conducted in vivo wherein the coupling between the stereociliary complex and the cupula is dictated by normal physiological factors. This may partially mask the influence of transduction adaptation revealed by stiff probe experiments in vitro, and may prevent the form of adaptation observed in vitro from occurring under physiological conditions (Vollrath and Eatock 2003).

Thus only the LG velocity-sensitive afferents have response dynamics that follow the cupular motion dictated by canal biomechanics. LG afferents have response dynamics analogous to the regularly discharging bouton afferents in the squirrel monkey, where it is not necessary to include an adaptation operator to describe the dynamics (Fernandez and Goldberg 1971; Goldberg and Fernandez 1971a,b; Hullar et al. 2004). Fish HG and A afferents and mammalian irregular afferents do not directly mimic hair-cell voltage temporal responses, but require an additional adaptation element to model their responses.

The difference between hair-cell and afferent responses is stark. Hair cells respond nearly in phase with angular head velocity and have gains that are nearly constant over the frequency bandwidth tested. Afferents, in contrast, have a wide variety of responses. Only the purely LG velocity-sensitive and mammalian regularly discharging afferents have temporal responses similar to those observed in hair cells. The very existence of velocity-sensitive

afferents, present in all species studied to date, indicates that at least a significant subset of hair cells would not be expected to exhibit appreciable adaptation under physiological conditions. Thus it is not surprising to find hair cells that do not adapt significantly. In contrast, many species have both nonadapting and adapting semicircular canal afferents similar to those reported here in the fish (Boyle and Highstein 1990; Brichta and Goldberg 1996; Dickman and Correia 1989b; Honrubia et al. 1989; O'Leary and Dunn 1976).

Present data show that signal processing must be interposed between the hair cell voltage and the afferent discharge to generate the wide range of observed afferent responses. This suggests that posttransduction current processing performed by pre- and/or postsynaptic sites is likely to participate in the generation of these dynamics. We note in passing that in 1996, Highstein et al. (1996) used endolymphatic polarization to elicit transmitter release from toadfish hair cells to distinguish pre- from posttransduction mechanisms. We and others (Brichta et al. 2002; Goldberg and Brichta 2002) cited the results of these studies to support the role of a pretransduction mechanism in shaping afferent response dynamics. However, in 1996 there was no data suggesting that there was diversity in hair cell transmitter phenotype, as we have recently demonstrated (Holstein et al. 2004a,c). Although the veracity of the 1996 data stands, they should now be reinterpreted considering that glutamatergic hair cells and GABAergic hair cells may not be equally resistive and may not respond equally to transepithelial voltage drops. Interpretation of the 1996 results in this light is consistent with the role we propose for hair cell–to– afferent synapses in shaping afferent diversity.

Synapses

Afferent response dynamics correlate with structural attributes of the distal neuritic processes and terminals (Boyle et al. 1991), lending support to the suggestion that a postsynaptic mechanism contributes to afferent signal processing. The dendritic arborizations and terminal endings are complex, particularly for HG and A afferents in fish (Boyle and Highstein 1990; Boyle et al. 1991) and for many mammalian irregular afferents (Lysakowski and Goldberg 1997; Lysakowski et al. 1995). Further complexity derives from the recent observation that hair cell transmitter phenotype is heterogeneous (Holstein et al. 2004b). Although most hair cells appear to use an excitatory amino acid such as glutamate, a small subset of canal hair cells is intensely GABA-immunoreactive (Fig. 9). GABAergic hair cells have also been demonstrated to be regionally distributed in the cristae of mice and pigeons (Holstein et al. 2004b). In fish, these GABAergic cells are present only in the central region of the crista (Holstein et al. 2004b,c), exactly where the acceleration-sensitive afferents terminate (Boyle and Highstein 1990; Boyle et al. 1991). Further, the HG and A afferents form synaptic contacts with both glutamatergic and GABAergic hair cells, whereas the LG afferents are innervated exclusively by glutamatergic hair cells (Holstein et al. 2004b,c). In Fig. 9, a topological comparison of the GABAergic hair cell locations in *A* and the locations of phase advanced afferents in *B* suggests that GABA may influence only those phase-advanced afferents. LG afferents, restricted to the crista periphery, are not distributed in the central region where GABAergic hair cells are localized, and thus should be free of the influence of these cells. Indeed A, but not LG, afferents were contacted on their dendritic tips by GABAergic cells (see Fig. 2 in Holstein et al. 2004c). To study potential GABAergic effects on afferent dynamics, we used systemic application of $GABA_A$ blockers while recording from afferents during recording and canal indentation. $GABA_A$ blockers were without effect. We then turned to the CGP class of compounds that specifically antagonize $GABA_B$ receptors. As seen in Fig. 10, shortly after the intraarteriolar injection of CGP 55845, the gain slope of the A-type afferent decreased from 0.89 to 0.55 and the phase was similarly retarded from acceleration toward velocity. These effects were most pronounced at stimulus frequencies <2 Hz and were not complete. That is, an acceleration-sensitive

afferent moved toward velocity sensitivity or a gain slope of zero. The *inset* reports the population response. These data support the role of synaptic transmission dynamics in shaping temporal responses of afferents.

We also studied afferent adaptation to step stimuli in the presence of CGP. Figure 11 illustrates that, after CGP administration, fast afferent adaptation did not change, but slow adaptation occurred over a longer extent of time. Again, the *inset* reflects a summary of the results of the adaptation changes associated with the administration of a $GABA_B$ antagonist, data consistent with changes observed in responses to sinusoidal stimuli. For complete results refer to Holstein et al. (2004b,c).

We suggest that the convergence of a fast excitatory and a slow inhibitory transmitter onto single afferents is responsible for part of the adaptation observed in phase-advanced (A-type) afferents. Blocking the slow transmitter results in a gain increase and phase decrease re: velocity <2 Hz as well as a decrease in the slow adaptation process to step stimuli. We hasten to note that these effects are only part of the differentiation process in vestibular afferents because they are present only at frequencies <2 Hz and do not reduce the phase of A-type afferents completely to velocity. This restriction to low frequencies is consistent with the expected time delay associated with a G protein–coupled receptor. Afferent temporal response diversity for stimulus frequencies >2 Hz, however, cannot be explained by this mechanism. Additionally, some afferents evidence a phase advance and gain slope that is nonzero even in the absence of GABAergic contacts and is particularly pronounced for stimuli >2 Hz. Therefore an additional factor must be present to account for temporal dynamics of these afferents.

FUTURE DIRECTIONS

All vertebrate species studied to date demonstrate afferents with temporal responses that reflect a form of adaptation or mathematical differentiation process. Convergence of excitatory and inhibitory synaptic inputs appears to play the major role at low frequencies (≲2 Hz; Holstein et al. 2004b,c), but the origin of fast adaptive responses has not yet been discovered. Holt et al. (2004) recorded miniature synaptic activity [miniature excitatory postsynaptic potentials (mEPSPs)] at these higher stimulus frequencies in bouton afferents of the turtle that exhibited temporal dynamics similar to that of the afferents. The mechanism by which canal hair cells release transmitter during the rising phase of hair cell voltage is certainly a rich area for future study. However, the Holt et al. quantal data, along with the hair cell voltage data summarized above, imply that the dynamic may be imparted by a yet-to-be-described hair cell presynaptic second messenger. Another area of future research involves high-frequency responses of the canals and the origins of spike timing. Canal afferents are capable of responding to stimuli at very high frequencies (Dickman and Correia 1989b;Rabbitt et al. 1995) and can exhibit phase-locking behavior similar to that of auditory afferents. Vestibular hair cells are known to resonate at certain frequencies in response to steps of current (Baird 1994;Correia and Lang 1990;Eatock et al. 1998;Goldberg and Brichta 2002;Rennie et al. 1996;Steinacker et al. 1992;Weng and Correia 1999). However, the correspondence between this hair cell electrical property and the output of the semicircular canal remains to be specified.

Acknowledgments

The authors are grateful to Drs. Victor Friedrich and Scott Henderson for assistance with image acquisition and processing.

GRANTS

This research was supported by National Institute on Deafness and Other Communication Disorders Grants P01 DC-01837 and R55 DC-05585.

REFERENCES

Baird RA. Comparative transduction mechanisms of hair cells in the bullfrog utriculus. I. Responses to intracellular current. J Neurophysiol 1994;71:666–684. [PubMed: 7909840]

Baird RA, Desmadryl G, Fernandez C, Goldberg JM. The vestibular nerve of the chinchilla. II. Relation between afferent response properties and peripheral innervation patterns in the semicircular canals. J Neurophysiol 1988;60:182–203. [PubMed: 3404216]

Blanks RH, Curthoys IS, Bennett ML, Markham CH. Planar relationships of the semicircular canals in rhesus and squirrel monkeys. Brain Res 1985;340:315–324. [PubMed: 3896405]

Blanks RH, Estes MS, Markham CH. Physiologic characteristics of vestibular first-order canal neurons in the cat. II. Response to constant angular acceleration. J Neurophysiol 1975;38:1250–1268. [PubMed: 809548]

Boyle R, Carey JP, Highstein SM. Morphological correlates of response dynamics and efferent stimulation in horizontal semicircular canal afferents of the toadfish, *Opsanus tau*. J Neurophysiol 1991;66:1504–1521. [PubMed: 1765791]

Boyle R, Highstein SM. Resting discharge and response dynamics of horizontal semicircular canal afferents of the toadfish, *Opsanus tau*. J Neurosci 1990;10:1557–1569. [PubMed: 2332797]

Bozovic D, Hudspeth AJ. Hair-bundle movements elicited by transepithelial electrical stimulation of hair cells in the sacculus of the bullfrog. Proc Natl Acad Sci USA 2003;100:958–963. [PubMed: 12538849]

Brichta AM, Aubert A, Eatock RA, Goldberg JM. Regional analysis of whole cell currents from hair cells of the turtle posterior crista. J Neurophysiol 2002;88:3259–3278. [PubMed: 12466445]

Brichta AM, Goldberg JM. Afferent and efferent responses from morphological fiber classes in the turtle posterior crista. Ann NY Acad Sci 1996;781:183–195. [PubMed: 8694414]

Brichta AM, Goldberg JM. Morphological identification of physiologically characterized afferents innervating the turtle posterior crista. J Neurophysiol 2000;83:1202–1223. [PubMed: 10712450]

Camis, M. The Physiology of the Vestibular Apparatus. Clarendon Press; Oxford, UK: 1930.

Correia MJ, Lang DG. An electrophysiological comparison of solitary type I and type II vestibular hair cells. Neurosci Lett 1990;116:106–111. [PubMed: 2259440]

Crawford AC, Evans MG, Fettiplace R. Activation and adaptation of transducer currents in turtle hair cells. J Physiol 1989;419:405–434. [PubMed: 2621635]

Curthoys IS. The response of primary horizontal semicircular canal neurons in the rat and guinea pig to angular acceleration. Exp Brain Res 1982;47:286–294. [PubMed: 7117453]

Curthoys IS, Oman CM. Dimensions of the horizontal semicircular duct, ampulla and utricle in the human. Acta Otolaryngol 1987;103:254–261. [PubMed: 3577757]

Damiano E, Rabbitt RD. A singular perturbation model of fluid dynamics in the vestibular semicircular canal and ampulla. J Fluid Mech 1996;307:333–372.

Dickman J. Spatial orientation of semicircular canals and afferent sensitivity vectors in pigeons. Exp Brain Res 1996;111:8–20. [PubMed: 8891631]

Dickman JD, Correia MJ. Responses of pigeon horizontal semicircular canal afferent fibers. I. Step, trapezoid, and low-frequency sinusoid mechanical and rotational stimulation. J Neurophysiol 1989a;62:1090–1101. [PubMed: 2585041]

Dickman JD, Correia MJ. Responses of pigeon horizontal semicircular canal afferent fibers. II. High-frequency mechanical stimulation. J Neurophysiol 1989b;62:1102–1112. [PubMed: 2585042]

Dickman JD, Reder PA, Correia MJ. A method for controlled mechanical stimulation of single semicircular canals. J Neurosci Methods 1988;25:111–119. [PubMed: 3172821]

Eatock RA, Rusch A, Lysakowski A, Saeki M. Hair cells in mammalian utricles. Otolaryngol Head Neck Surg 1998;119:172–181. [PubMed: 9743073]

Estes MS, Blanks RH, Markham CH. Physiologic characteristics of vestibular first-order canal neurons in the cat. I. Response plane determination and resting discharge characteristics. J Neurophysiol 1975;38:1232–1249. [PubMed: 1177015]

Ewald, JR. Physiologish Untersuchingen über das Endorgan des Nervs Octavus. Bergmann; Wiesbaden, Germany: 1892.

Fernandez C, Baird RA, Goldberg JM. The vestibular nerve of the chinchilla. I. Peripheral innervation patterns in the horizontal and superior semicircular canals. J Neurophysiol 1988;60:167–181. [PubMed: 3404215]

Fernandez C, Goldberg JM. Physiology of peripheral neurons innervating semicircular canals of the squirrel monkey. II. Response to sinusoidal stimulation and dynamics of peripheral vestibular system. J Neurophysiol 1971;34:661–675. [PubMed: 5000363]

Fernandez C, Goldberg JM, Baird RA. The vestibular nerve of the chinchilla. III. Peripheral innervation patterns in the utricular macula. J Neurophysiol 1990;63:767–780. [PubMed: 2341875]

Fernandez C, Lysakowski A, Goldberg JM. Hair-cell counts and afferent innervation patterns in the cristae ampullares of the squirrel monkey with a comparison to the chinchilla. J Neurophysiol 1995;73:1253–1269. [PubMed: 7608769]

Fettiplace R, Ricci AJ. Adaptation in auditory hair cells. Curr Opin Neurobiol 2003;13:446–451. [PubMed: 12965292]

Goldberg JM. Afferent diversity and the organization of central vestibular pathways. Exp Brain Res 2000;130:277–297. [PubMed: 10706428]

Goldberg JM, Brichta AM. Evolutionary trends in the organization of the vertebrate crista ampullaris. Otolaryngol Head Neck Surg 1998;119:165–171. [PubMed: 9743072]

Goldberg JM, Brichta AM. Functional analysis of whole cell currents from hair cells of the turtle posterior crista. J Neurophysiol 2002;88:3279–3292. [PubMed: 12466446]

Goldberg JM, Fernandez C. Physiology of peripheral neurons innervating semicircular canals of the squirrel monkey. III. Variations among units in their discharge properties. J Neurophysiol 1971a; 34:676–684. [PubMed: 5000364]

Goldberg JM, Fernandez C. Physiology of peripheral neurons innervating semicircular canals of the squirrel monkey. I. Resting discharge and response to constant angular accelerations. J Neurophysiol 1971b;34:635–660. [PubMed: 5000362]

Goldberg JM, Fernandez C. Responses of peripheral vestibular neurons to angular and linear accelerations in the squirrel monkey. Acta Otolaryngol 1975;80:101–110. [PubMed: 809987]

Goldberg JM, Lysakowski A, Fernandez C. Morphophysiological and ultrastructural studies in the mammalian cristae ampullares. Hear Res 1990;49:89–102. [PubMed: 2292511]

Goldberg JM, Lysakowski A, Fernandez C. Structure and function of vestibular nerve fibers in the chinchilla and squirrel monkey. Ann NY Acad Sci 1992;656:92–107. [PubMed: 1599221]

Goldberg JM, Smith CE, Fernandez C. Relation between discharge regularity and responses to externally applied galvanic currents in vestibular nerve afferents of the squirrel monkey. J Neurophysiol 1984;51:1236–1256. [PubMed: 6737029]

Highstein S, Politoff A. Relation of interspike baseline activity to the spontaneous discharges of primary afferents from the labyrinth of the toadfish, *Opsanus tau*. Brain Res 1978;150:182–187. [PubMed: 208713]

Highstein SM, Rabbitt RD, Boyle R. Determinants of semicircular canal afferent response dynamics in the toadfish, *Opsanus tau*. J Neurophysiol 1996;75:575–596. [PubMed: 8714636]

Hille, B. Ionic Channels of Excitable Membranes. Sinauer Associates; Sunderland, MA: 1992.

Hillman DE, McLaren JW. Displacement configuration of semicircular canal cupulae. Neuroscience 1979;4:1989–2000. [PubMed: 316877]

Holstein GR, Martinelli GP, Boyle R, Rabbitt RD, Highstein SM. Ultrastructural observations of efferent terminals in the crista ampullaris of the toadfish, *Opsanus tau*. Exp Brain Res 2004a; 155:265–273. [PubMed: 14689144]

Holstein GR, Martinelli GP, Henderson SC, Friedrich VL Jr, Rabbitt RD, Highstein SM. gamma-Aminobutyric acid is present in a spatially discrete subpopulation of hair cells in the crista ampullaris of the toadfish *Opsanus tau*. J Comp Neurol 2004b;471:1–10. [PubMed: 14983471]

Holstein GR, Rabbitt RD, Martinelli GP, Friedrich VL Jr, Boyle RD, Highstein SM. Convergence of excitatory and inhibitory hair cell transmitters shapes vestibular afferent responses. Proc Natl Acad Sci USA 2004c;101:15766–15771. [PubMed: 15505229]

Holt, C.; Xue, J.; Goldberg, J. Stimulated Synaptic Activity in Bouton Afferents of the Turtle Posterior Crista. Abstracts of the Association for Research in Otolaryngology; Daytona Beach, FL: 2004. p. 1566

Holt JR, Corey DP, Eatock RA. Mechanoelectrical transduction and adaptation in hair cells of the mouse utricle, a low-frequency vestibular organ. J Neurosci 1997;17:8739–8748. [PubMed: 9348343]

Honrubia V, Hoffman LF, Sitko S, Schwartz IR. Anatomic and physiological correlates in bullfrog vestibular nerve. J Neurophysiol 1989;61:688–701. [PubMed: 2786056]

Honrubia V, Sitko S, Kimm J, Betts W, Schwartz I. Physiological and anatomical characteristics of primary vestibular afferent neurons in the bullfrog. Int J Neurosci 1981;15:197–206. [PubMed: 6172398]

Hudspeth AJ. How the ear's works work. Nature 1989a;341:397–404. [PubMed: 2677742]

Hudspeth AJ. Mechanoelectrical transduction by hair cells of the bullfrog's sacculus. Prog Brain Res 1989b;80:129–135. discussion 127–128. [PubMed: 2699361]

Hudspeth AJ. How hearing happens. Neuron 1997;19:947–950. [PubMed: 9390507]

Hullar TE, Lasker DM, Hirvonen TP, Carey JP, Minor LB. High-frequency sinusoidal stimulation of irregularly discharging vestibular-nerve afferents: linear response. J Neurophysiol. In press.

Igarashi M. Architecture of the otolith end organ: some functional considerations. Ann Otol Rhinol Laryngol 1966;75:945–955. [PubMed: 4959679]

Igarashi M, Yoshinobu T. Comparative observations of the eminentia cruciata in birds and mammals. Anat Rec 1966;155:269–277. [PubMed: 4960422]

Johansson RS, Valbo AB. Tactile sensory coding in the glabrous skin of the human hand. Trends Neurosci 1983;1:27–33.

Kennedy HJ, Evans MG, Crawford AC, Fettiplace R. Fast adaptation of mechanoelectrical transducer channels in mammalian cochlear hair cells. Nat Neurosci 2003;6:832–836. [PubMed: 12872124]

Kernell D. The repetitive impulse discharge of a simple neurone model compared to that of spinal motoneurones. Brain Res 1968;11:685–687. [PubMed: 5712015]

Landolt JP, Correia MJ. Neurodynamic response analysis of anterior semicircular canal afferents in the pigeon. J Neurophysiol 1980;43:1746–1770. [PubMed: 6251181]

Liberman MC. Single-neuron labeling in the cat auditory nerve. Science 1982;216:1239–1241. [PubMed: 7079757]

Lorenté de Nó R. Contribucion al estudio matematico del organo del equilibrio. Trabajo publicado en la 1927;7:202–206.

Lowenstein O, Sand A. The mechanism of semi-circular canals: a study of single fiber preparations to angular acceleration and to rotation at constant speed. Proc R Soc Lond B Biol Sci 1940;129:256–275.

Lysakowski A, Goldberg JM. A regional ultrastructural analysis of the cellular and synaptic architecture in the chinchilla cristae ampullares. J Comp Neurol 1997;389:419–443. [PubMed: 9414004]

Lysakowski, A.; Goldberg, JM. Morphophysiology of the vestibular periphery. In: Highstein, SM.; Popper, A.; Fay, R., editors. The Vestibular System. Springer-Verlag; New York: 2004.

Lysakowski A, Minor LB, Fernandez C, Goldberg JM. Physiological identification of morphologically distinct afferent classes innervating the cristae ampullares of the squirrel monkey. J Neurophysiol 1995;73:1270–1281. [PubMed: 7608770]

Norris CH, Miller AJ, Perin P, Holt JC, Guth PS. Mechanisms and effects of transepithelial polarization in the isolated semicircular canal. Hear Res 1998;123:31–40. [PubMed: 9745953]

O'Leary DP, Dunn RF. Analysis of afferent responses from isolated semicircular canal of the guitarfish using rotational acceleration white-noise inputs. I. Correlation of response dynamics with receptor innervation. J Neurophysiol 1976;39:631–644. [PubMed: 948010]

O'Leary DP, Dunn RF, Honrubia V. Functional and anatomical correlation of afferent responses from the isolated semicircular canal. Nature 1974;251:225–227. [PubMed: 4424704]

Rabbitt RD, Boyle R, Highstein SM. Mechanical indentation of the vestibular labyrinth and its relationship to head rotation in the toadfish, *Opsanus tau*. J Neurophysiol 1995;73:2237–2260. [PubMed: 7666136]

Rabbitt RD, Boyle R, Highstein SM. Influence of surgical plugging on horizontal semicircular canal mechanics and afferent response dynamics. J Neurophysiol 1999;82:1033–1053. [PubMed: 10444695]

Rabbitt RD, Boyle R, Holstein GR, Highstein SM. Hair-cell versus afferent adaptation in the semicircular canals. J Neurophysiol 2005;93:424–436. [PubMed: 15306633]

Rabbitt, RD.; Damiano, ER.; Grant, JW. Biomechanics of the semicircular canals and otolith organs. In: Highstein, SM.; Popper, A.; Fay, R., editors. The Vestibular System. Springer-Verlag; New York: 2004.

Reisine H, Simpson JI, Henn V. A geometric analysis of semicircular canals and induced activity in their peripheral afferents in the rhesus monkey. Ann NY Acad Sci 1988;545:10–20. [PubMed: 2853588]

Rennie KJ, Ricci AJ, Correia MJ. Electrical filtering in gerbil isolated type I semicircular canal hair cells. J Neurophysiol 1996;75:2117–2123. [PubMed: 8734607]

Ricci AJ, Crawford AC, Fettiplace R. Active hair bundle motion linked to fast transducer adaptation in auditory hair cells. J Neurosci 2000;20:7131–7142. [PubMed: 11007868]

Ricci AJ, Wu YC, Fettiplace R. The endogenous calcium buffer and the time course of transducer adaptation in auditory hair cells. J Neurosci 1998;18:8261–8277. [PubMed: 9763471]

Schessel DA, Ginzberg R, Highstein SM. Morphophysiology of synaptic transmission between type I hair cells and vestibular primary afferents. An intracellular study employing horseradish peroxidase in the lizard, *Calotes versicolor*. Brain Res 1991;544:1–16. [PubMed: 1713111]

Shepherd, GM.; Corey, DP. Sensational science. New Biol; Sensory Transduction: 45th Annual Symposium of the Society of General Physiologists, Marine Biological Laboratory; Woods Hole, MA. September 5–8, 1991; 1992. p. 48-52.

Shepherd GM, Corey DP. The extent of adaptation in bullfrog saccular hair cells. J Neurosci 1994;14:6217–6229. [PubMed: 7931574]

Silver RB, Reeves AP, Steinacker A, Highstein SM. Examination of the cupula and stereocilia of the horizontal semicircular canal in the toadfish *Opsanus tau*. J Comp Neurol 1998;402:48–61. [PubMed: 9831045]

Smotherman MS, Narins PM. Hair cells, hearing and hopping: a field guide to hair cell physiology in the frog. J Exp Biol 2000;203:2237–2246. [PubMed: 10887064]

Spoor F, Bajpai S, Hussain ST, Kumar K, Thewissen JG. Vestibular evidence for the evolution of aquatic behaviour in early cetaceans. Nature 2002;417:163–166. [PubMed: 12000957]

Steinacker A, Monterrubio J, Perez R, Highstein SM. Potassium current composition and kinetics in toadfish semicircular canal hair cells. Biol Bull 1992;183:346–347.

Steinhausen W. Über die beobachtungen der cupula in der bognegangsampullen des labyrinthes des libenden hecths. Pfluegers Arch 1933;232:500–512.

Van Buskirk WC, Watts RG, Liu YK. The fluid mechanics of the semicircular canals. J Fluid Mech 1976;78:87–98.

Vollrath MA, Eatock RA. Time course and extent of mechanotransducer adaptation in mouse utricular hair cells: comparison with frog saccular hair cells. J Neurophysiol 2003;90:2676–2689. [PubMed: 12826658]

Walsh BT, Miller JB, Gacek RR, Kiang NYS. Spontaneous activity in the eighth cranial nerve of the cat. Int J Neurosci 1972;3:221–236.

Weng T, Correia MJ. Regional distribution of ionic currents and membrane voltage responses of type II hair cells in the vestibular neuroepithelium. J Neurophysiol 1999;82:2451–2461. [PubMed: 10561418]

Wersäll, J.; Bagger-Sjöbäck, D. Morphology of vestibular sense organ. In: Kornhuber, HH., editor. Handbook of Sensory Physiology, Vestibular System, Basic Mechanisms. Vol. vol. 6. Springer-Verlag; Berlin: 1974. p. 123-170.

Wu YC, Ricci AJ, Fettiplace R. Two components of transducer adaptation in auditory hair cells. J Neurophysiol 1999;82:2171–2181. [PubMed: 10561397]

Yamauchi A, Highstein SM, King C, Rabbitt RD, Boyle D. Displacement of the semicircular canal cupula for sinusoidal stimuli. Assoc Res Otolaryngol Abstr 2002a;125

Yamauchi A, Rabbitt RD, Boyle R, Highstein SM. Relationship between inner-ear fluid pressure and semicircular canal afferent nerve discharge. J Assoc Res Otolaryngol 2002b;3:26–44. [PubMed: 12083722]

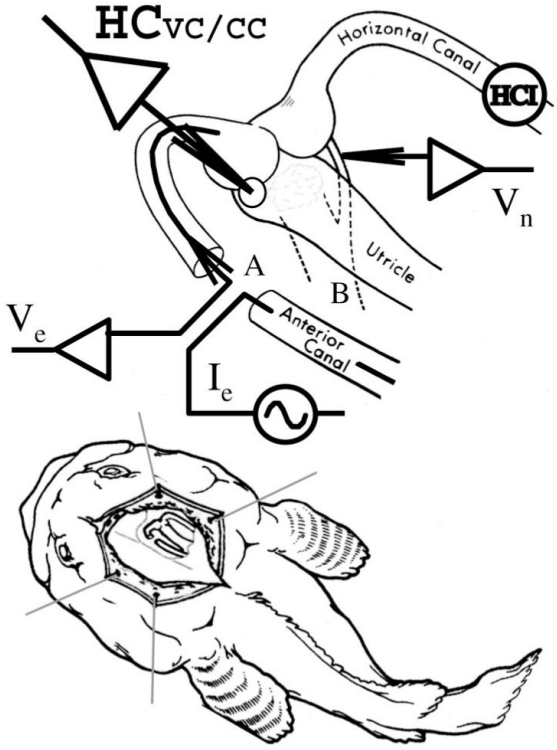

FIG. 1.

General experimental setup. *Top*: expanded view of the labyrinth. *Bottom*: overview of the fish. A current-passing electrode (I_e) is placed in the posterior limb of the anterior canal and a second voltage-measuring electrode (V_e) placed in the anterior canal ampulla for applying and recording electrical polarization stimuli, respectively. Mechanical stimulation of the horizontal semicircular canal is provided by a piezo electrically driven indenter placed on the long and slender limb of the canal duct (HCI); this mode of canal activation can be tailored to closely mimic head rotation but can be applied independent of head movement in space. Extracellular afferent records (V_n) were obtained simultaneously with the applied stimuli. A small hole was made in the utricular side of the horizontal canal ampulla for access to the sensory epithelium by sharp electrodes to record hair cell receptor potentials or currents during canal indentation or polarization or a combination of the 2 stimuli.

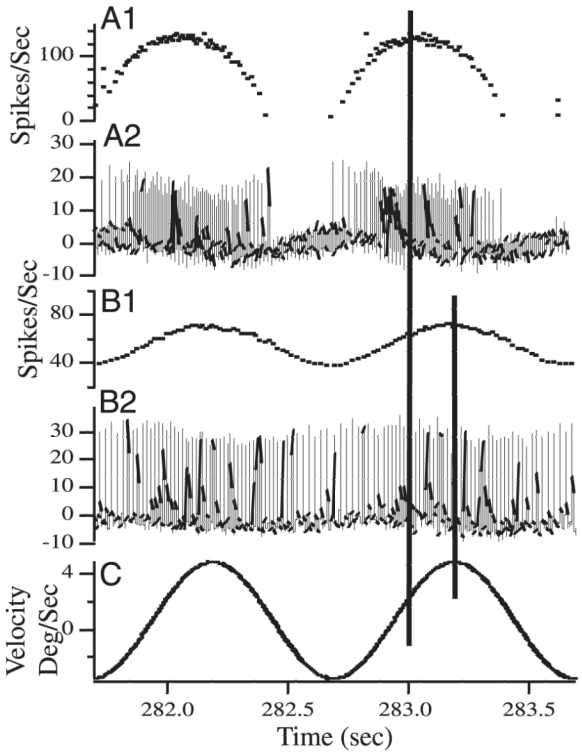

FIG. 2.

Primary afferent records during canal indentation. A_2 and B_2 are raw spike records and C is the magnitude of the indenter stimulus quantitated as degrees/s (cf. Rabbitt et al. 1995). A_1 and B_1 are instantaneous firing histograms of A_2 and B_2, respectively, in spikes/s. Vertical line to the *right* is aligned on peak discharge in B_1 and crosses the stimulus velocity at peak velocity. Therefore the spike peak discharge indicated in B_1 is *in-phase* with peak stimulus velocity. Vertical line to the *left* is aligned with peak discharge in A_1 and crosses the stimulus velocity profile near peak acceleration. Therefore the cell in *A* is *in-phase* with acceleration.

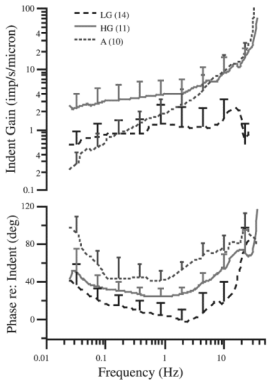

FIG. 3.

Summary of afferent responses to canal indentation. Dashed line: afferents are grouped according to gain and phase into low gain (LG); solid line: high gain (HG); short dashed line: acceleration (A). Error bars show SDs associated with interafferent variability within each group and thus span the region between the average curves. Replotted from Highstein et al. (1996).

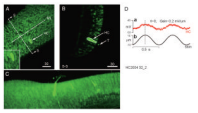

FIG. 4.

Characterized and labeled hair cell. Cells were characterized physiologically using mechanical stimuli, injected, and visualized using streptavidin-Alexafluor 568 and multiphoton microscopy. *A*: maximum intensity projected image showing the location of an injected hair cell (HC) in the central region of the crista (scale bars: 30 μm). Approximate locations of the midline (ML) and center (SS) are indicated. Background staining is biotin, normally present in the cells, and recognized by the streptavidin. *B*: a single optical slice showing the same hair cell viewed in the direction SS perpendicular to the ML. *C*: a rotated, rendered maximum intensity projected image in which the presence of tracer in the hair bundle is clear. *D*: response of the same cell to a ±10-μm sinusoidal mechanical indentation (*b*) of the canal duct at 2 Hz. Voltage modulation of this cell in current clamp (*a*) was in phase with the stimulus and the gain was 0.2 mV/μm indent.

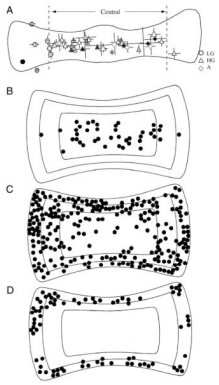

FIG. 5.

Location of the dendritic fields in the crista ampularis of the toadfish (*A*, after Boyle et al. 1991) and the chinchilla (*B–D*, after Fernandez et al. 1988). In *A* circles represent LG, triangles HG, and diamonds A units. Relative center of each field is plotted on a normalized crista. Dotted vertical lines indicate the central 2/3rds of the crista containing the HG and A afferents. *B*: location of 41 calyx units. *C*: 248 dimorphic units. *D*: 79 bouton units. Solid lines indicate the approximate boundaries of the central, intermediate, and peripheral zones of the crista.

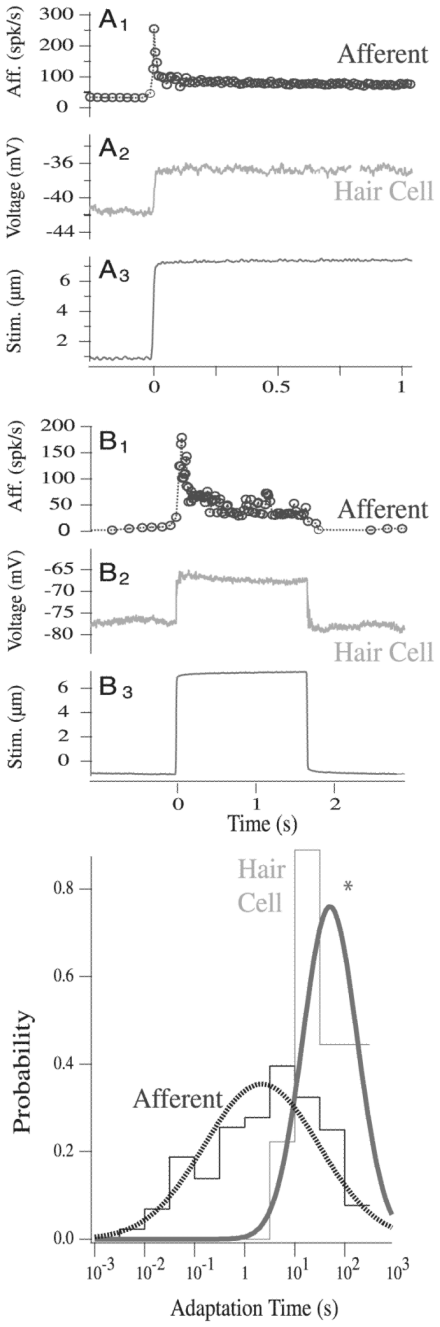

FIG. 6.

Primary afferent and hair cell adaptation to step indentation stimuli. Example records showing slowly adapting (dots, A_1) and rapidly adapting (dots, B_1) afferents in response to step stimuli (solid, A_3, B_3) in the plug canal condition. Afferent discharge adaptation for excitatory stimuli was fit using a double-exponential curve (slow and fast time constants τ_s, τ_f) and using a single exponential for inhibitory stimuli (slow time τ_s). A_2 and B_2 are example records of hair cell responses to the same steps. Records were not obtained simultaneously. To the *right* are histograms and curve fits of afferent and hair cell adaptation probabilities. Afferent adaptation times spanned approximately 6 orders of magnitude, whereas hair cell adaptation times were more limited.

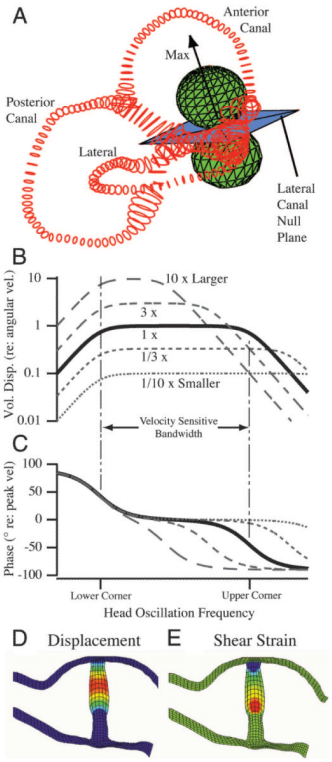

FIG. 7.

Semicircular canal mechanics. *A*: reconstruction of the human membranous labyrinth (red) and corresponding maximal response direction (arrow) and null-plane for the lateral canal (Rajguru et al. 2004). *B–C*: cupula volume displacement shown as magnitude (*B*) and phase (*C*) vs. frequency of angular head oscillation. Results are shown normalized relative to peak angular velocity for several different sized labyrinths. *D–E*: cross section through the ampulla showing displacement (*D*) and shear strain in the cupula (*E*) leading to hair bundle activation for low-frequency head movements (max = red, min = blue).

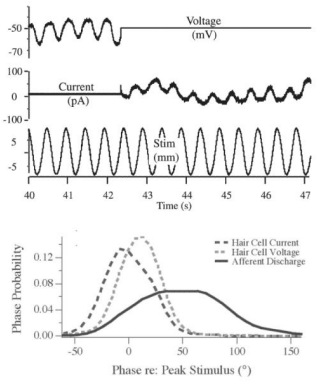

FIG. 8.

Receptor voltage and current clamp responses to sinusoidal indentation. *Top line*: receptor potentials in current clamp and the 2nd line receptor currents in voltage clamp in response to sinusoidal indentation illustrated on the 3rd line. Note that the clamp was switched from current clamp to voltage clamp after the 5th cycle of indentation. Zero current potential for this hair cell was about −50 mV. *Bottom plot*: probability function of the receptor current, receptor potential, and afferent phases to the indentational stimuli. Note that the phase spanned by the afferents is several orders greater than that of the hair cells.

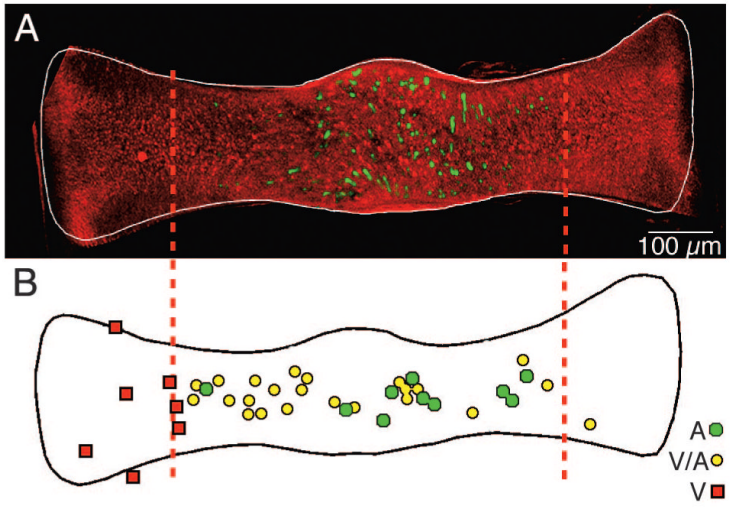

FIG. 9.

Topography of GABAergic hair cells. *A*: low-magnification multiphoton laser scanning projected image showing the spatially restricted distribution of GABAergic hair cells (Alexa 488, green) in relation to the ubiquitous glutamatergic hair cells (Alexa 568, red) across an entire crista ampullaris of a double-labeled canal crista. Vertical dashed lines demarcate the central 60% of the crista. *B*: locations of dendritic fields of 38 physiologically characterized, labeled afferents. Relative center of each dendritic field for pure velocity-sensitive (V, red squares), mixed velocity-acceleration sensitive (V-A, yellow circles), and acceleration-sensitive (A, green circles) afferents are plotted on a normalized crista (after Boyle et al. 1991). GABA-immunofluorescent hair cells (Alexafluor-488; green) visualized by multiphoton laser scanning microscopy in a whole mount of a toadfish horizontal canal crista. GABAergic hair cells are present only in the central region of the sensory epithelium. [Figure 9 originally published in PNAS USA 101: 15766 –71, copyright © 1993–2004 by The National Academy of Sciences of the United States of America, all rights reserved.]

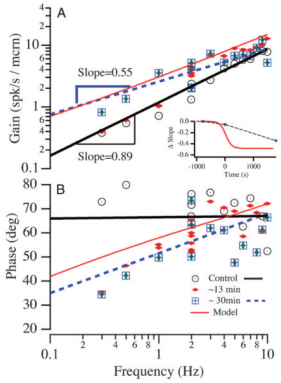

FIG. 10.

Bode plots of log gain (*A*, spikes per s per μm of canal indentation) and phase (*B*, spikes/s re: peak amplitude of stimulation) vs. log frequency of stimulation for a single high-α afferent before and after CGP 55845 injection at 400 μg. Different symbols correspond to measurements obtained 13 and 30 min postinjection. Gain slopes are indicated for the linear fits of the data. Gain slope is plotted overlying that of the suction electrode experiments in *A*. *Inset*: 2-transmitter convergence model (Holstein et al. 2004c) was used to predict how the unit in the control condition (thick black solid line) would be expected to respond after $GABA_B$ receptor blockade (thin red curved lines). Note correspondence between the predicted response (red curved lines) and the postdrug data (dashed line curve fits). [Figure 10 originally published in PNAS 101: 15766 –71, copyright © 1993–2004 by The National Academy of Sciences of the United States of America, all rights reserved.]

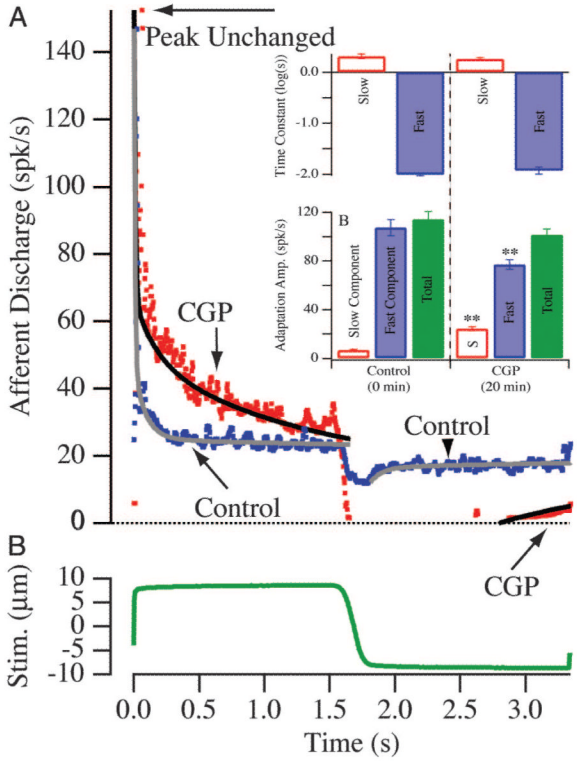

FIG. 11.

Afferent adaptation to step excitatory and inhibitory stimuli (step amplitude indicated in *B*) of a mixed velocity-acceleration afferent. Afferent discharge adaptation for excitatory stimuli was fit by using a double-exponential curve (slow and fast time constants τ_s, τ_f) and a single exponential for inhibitory stimuli (slow time τ_s). *Inset*: summary statistics of afferent adaptation changes associated with $GABA_B$ receptor administration. Data were fit as double exponentials by using: spikes/s = $A_0 + A_1e^{-t/\tau 1} + A_2e^{-t/\tau 2}$. τ_1 is the fast time constant, τ_2 is the slow time constant, A_1 is the fast component amplitude, A_2 is the slow component amplitude, and $A_1 + A_2$ is the total adaptation amplitude. Error bars denote SE. There was no statistically significant change in τ_1 or τ_2, but significant differences were observed in the relative proportions of A_1 and A_2 (** denotes 0.05 level) such that total time required to recovery lengthened after CGP administration. [Figure 11 originally published in PNAS 101: 15766 –71, copyright © 1993–2004 by The National Academy of Sciences of the United States of America, all rights reserved.]